

The singlet-triplet and exchange-only flopping-mode spin qubits

Simon Stastny and Guido Burkard

Department of Physics, University of Konstanz, D-78457, Konstanz, Germany

Semiconductor-based spin qubits embedded into a superconducting microwave cavity constitute a fast-progressing and promising platform for realizing fast and fault-tolerant qubit control with long-range two-qubit coupling. The flopping-mode spin qubit consists of a single electron in a double quantum dot; it combines a charge qubit with a spin qubit. With its strong and tunable cavity coupling, the flopping-mode qubit is proven to be well-suited for low-power qubit control and cavity-mediated long-range quantum gates. The singlet-triplet (ST) and exchange-only (EO) qubits are multi-electron realizations that go without broadband control and are protected from some types of noise, but are challenging to couple to each other and to microwave cavities. We combine the flopping-mode concept with the ST and EO qubits and propose two new flopping-mode qubits that consist of three (four) quantum dots, occupied by two (three) electrons near the $(1, 0, 1) \leftrightarrow (0, 1, 1)$ [$(1, 0, 1, 1) \leftrightarrow (0, 1, 1, 1)$] charge transition. The two-electron system augments the ST_0 spin qubit with a charge qubit that interacts transversally and longitudinally with a cavity. Both couplings are highly tunable, and the longitudinal coupling distinguishes the flopping-mode ST qubit from the regular flopping-mode qubit. The longitudinal coupling allows for non-dissipative universal control similar to superconducting transmon qubits. The EO flopping-mode qubit comprises four dots occupied by three electrons and opens a new possibility to perform two-qubit gates for EO qubits that are challenging to perform directly with the exchange coupling. We use input-output theory to provide means of extracting the coupling strengths from cavity transmission data.

I. INTRODUCTION

Spin qubits in semiconductor quantum dots (QDs) [1] are a promising platform for quantum computation and have called a flourishing research field into action. The absence of a nuclear spin in ^{28}Si allows for qubits with remarkably long coherence times [2, 3] and quantum gates with error rates in the range or below typical error thresholds for fault-tolerant quantum computation [4].

Various qubit encodings beyond the single-spin (Loss-DiVincenzo) qubit have been realized within this platform, such as the singlet-triplet (ST_0) qubit [5–7] and the exchange-only (EO) qubit [8–13]. These encodings require more than one quantum dot for each qubit, and in return allow for partial or complete electric baseband control, thus relaxing the requirements regarding high-frequency driving or inhomogeneous magnetic fields. In addition, the EO qubit allows for complete control using only the exchange interaction [8, 14]. However, this simplification comes with a substantial complexity of the implementation of exchange-based two-qubit gates [8, 9, 15].

Universal quantum computing requires non-local two-qubit gates, in addition to the nearest-neighbor gates that can be directly implemented with the exchange interaction. Multi-spin exchange-coupled quantum dot systems can also be used to realize a spin bus, a spin chain which can be used as an intermediate-range two-qubit coupling [16–19]. Moreover, super-exchange can be used to couple two spin qubits by placing them next to a mediator unit, (virtual) excitations of which can mediate an indirect exchange interaction between the spins of interest [20, 21]. Long-range interactions between EO qubits are hard to realize, as the exchange interaction only couples nearest neighbor spins [22]. Spin shuttling is an effective way of

realizing non-local spin-spin interactions by transporting spins with a modulating confinement field [23, 24].

Much longer-range interactions between spin qubits may be achievable by leveraging the interactions between localized spins and delocalized cavity photons in a superconducting microwave cavity [25]. To achieve sufficiently large spin-photon couplings, substantial electric dipole couplings are required. Although the two-electron ST qubit and the three-electron EO qubit possess an electric dipole near a $(1,1)$ - $(0,2)$ or $(1,1,1)$ - $(1,0,2)$ charge transition [26–30], the corresponding dipoles are relatively small. However, by adding an empty dot, charge-like degrees of freedom (charge qubits) can be integrated into spin-qubit systems. A paradigmatic example of such a spin-charge qubit system is the flopping-mode spin qubit [31, 32] which extends the Loss-DiVincenzo (LD) qubit to one electron in two dots, and lends itself to the realization of fast long-range interactions without charge transport. Due to the exchange of virtual photons, distant two-qubit operations can be realized [33, 34]. The coupling can be achieved because the charge-like qubit can couple to the electric field of a superconducting cavity, and establish coherent photon charge interactions. Then, due to an artificial spin-orbit interaction, photon-spin interactions can arise [35–40], allowing for non-local two-qubit gates [41].

By injecting a probe field into the cavity and measuring the output field, cavity QED can also be used to measure these couplings, or to perform a dispersive readout of the qubit states [42–46]. In the case of the flopping-mode spin qubit [38, 47–49] the experimental realization was successful [50], and entanglement between two cavity-coupled qubits has been measured. [48]. Electrically tunable tunneling and detuning of the dots give the system a dipole moment and a magnetic field gradient between the

dots gives rise to the spin-orbit coupling. This flopping-mode qubit thus is a mechanism of making spin qubits like the LD qubit ‘charge like’. The question arises as to whether this is possible for more general spin qubits such as the more noise resistant delocalized multi electron ST_0 - or EO-spin qubits, i.e., whether the ST and EO qubits can be made ‘charge like’ in this way, by coupling them to an additional unoccupied quantum dot. In this paper, we introduce two new spin-qubit flavors that combine the flopping-mode qubit with the ST_0 and the EO qubits and inherit some of the favorable properties of both concepts.

This is done by equipping the singlet-triplet qubit and the EO qubit with an additional, unoccupied quantum dot. Starting from the ST_0 qubit, the resulting qubit then consists of three quantum dots in a magnetic field gradient. The system operates near the $(0, 1, 1) \leftrightarrow (1, 0, 1)$ charge transition, endowing it with an electric dipole moment. Such an arrangement can also be used for a cavity-based measurement of the exchange interaction in adjacent quantum dots [51]. The flopping-mode EO qubit comprises four quantum dots in a global Zeeman field. Charge hybridization between the $(0, 1, 1, 1)$, $(1, 0, 1, 1)$, and $(1, 1, 0, 1)$ charge states provides the qubit with an electric dipole moment. With this approach, one can use the advantages of these two qubit types, while achieving a tunable transversal and longitudinal cavity coupling. Especially longitudinal coupling is a promising feature as it is not subject to the Purcell effect and has already been investigated both in superconducting systems such as transmon qubits [52–55] and in spin qubits embedded in superconducting cavities [56, 57]. Moreover, as we will show, the longitudinal coupling enables a coupling of the EO subsystem (rather than subspace) qubit to cavity photons.

Recently, a similar system, consisting of a triple quantum dot occupied with two electrons has been studied in [18, 58]. These works investigate the use of the system as two qubits, a single LD qubit and a flopping-mode qubit, that can couple locally, while the flopping-mode qubit is coupled to a resonator.

The remainder of this paper is structured as follows: In Section II we introduce the model and we investigate and derive an effective qubit Hamiltonian for the flopping-mode ST qubit. In Section III we analyze the spin-photon couplings from the effective Hamiltonian. In Section IV we derive an equation for the cavity transmission and phase and propose an experiment to obtain the spin-photon couplings by analyzing these two quantities. We consider the flopping-mode EO qubit in Section V. Finally, we summarize our results in Section VI.

II. MODEL OF THE SINGLET-TRIPLET FLOPPING-MODE QUBIT

The starting point of our model is the flopping-mode qubit [38], consisting of one electron in a double quantum dot, see Fig. 1(a), with both dots in a global Zeeman

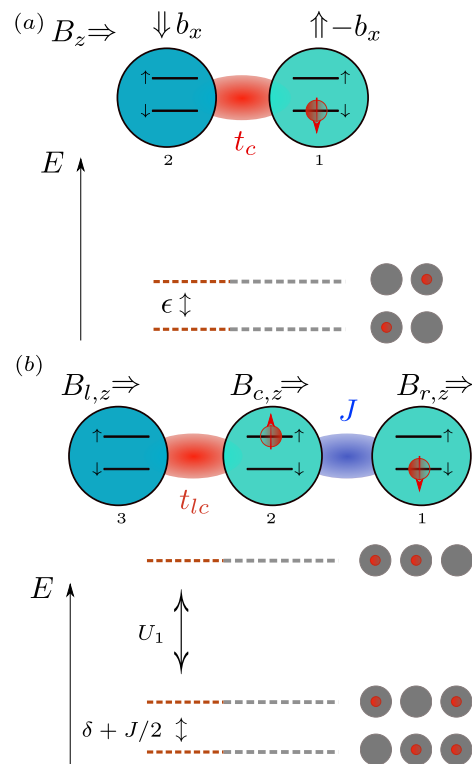


Figure 1. *Flopping-mode spin qubits.* (a) Schematics and charge energy levels of the (single-spin) flopping-mode qubit. A double quantum dot (DQD) occupied by one electron is placed in a global Zeeman field B_z in the chosen z -direction. A perpendicular magnetic field gradient b_x in x -direction is applied. The tunnel coupling t_c and the field gradient induce an effective (synthetic) spin-orbit (SO) coupling. An energy splitting of the two charge states can be achieved by detuning the two dots by ϵ . If $|\epsilon| \gg |t_c|$, the electron is confined in one dot, effectively acting as an LD qubit. If $|\epsilon| \ll |t_c|$, the electron is delocalized, thus allowing for SO-coupling (flopping mode). (b) The proposed singlet-triplet flopping-mode qubit. A third dot (3) is attached to a singlet-triplet qubit (dots 1 and 2). Local magnetic fields $B_{i,z}$ are applied to the three dots and form a field gradient. One of the three charge states is separated by the nearest-neighbor Coulomb repulsion energy U_1 , the other two again form an effective flopping-mode qubit, detuned by $\delta + J/2 \ll U_1$.

field B_z . The electron can tunnel between the two ground state orbitals of the dots, with tunnel matrix element t_c . A perpendicular local magnetic field gradient $\Delta b = 2b_x$ is applied to realize spin-orbit hybridization. The ground state energies of the dots differ by an energy ϵ . With the electron spin $\mathbf{S} = \frac{1}{2}\boldsymbol{\sigma}$ and the charge degree of freedom $\boldsymbol{\tau}$, the Hamiltonian for this model is given by

$$H_{\text{fm},1} = \frac{\epsilon}{2}\tau_z + t_c\tau_x + \frac{B}{2}\sigma_z + \frac{\Delta b}{2}\sigma_x\tau_z + g_c\tau_z(a + a^\dagger), \quad (1)$$

where τ_x and τ_z are Pauli matrices defined in the $|L, R\rangle$ basis, while σ_x and σ_z are Pauli matrices for the electron spin. The last term describes the coupling of the charge to

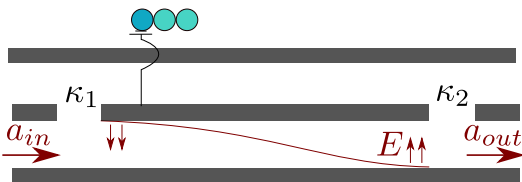


Figure 2. *Schematics of the cavity setup.* The cavity can leak at the two exit ports 1 and 2 with leakage rates κ_1 and κ_2 . The third quantum dot of the singlet-triplet flopping-mode qubit is coupled to the voltage at the center conductor of the cavity at an antinode of the electric field E (near port 1). The cavity is probed by injecting a microwave tone a_{in} and observing the transmitted signal a_{out} . The electric-field profile E is indicated in red.

a microwave cavity mode with coupling strength g_c . The charge parameters ϵ and t_c are electrically tunable and determine the effective spin-photon coupling [38]. The maximum g_c is reached at the charge sweet spot where $\epsilon = 0$. The flopping-mode qubit can be seen as an LD qubit [1] extended by an additional tunnel-coupled empty dot that enables spin-photon coupling. We extend this idea of the flopping-mode qubit to the singlet-triplet ST_0 qubit [7] by adding an empty dot. The ST_0 qubit is realized by two exchange-coupled quantum dots occupied by one electron each, immersed into an inhomogeneous magnetic (Zeeman) field. To apply the ‘flopping-mode mechanism’, i.e., endow this qubit with an electric dipole moment, this ST_0 qubit is coupled to a third, empty quantum dot. The resulting model consists of three quantum dots occupied by a total of two electrons, see Fig. 1(b). The local Zeeman field at each dot $j \in \{l, c, r\}$ is denoted as $B_{z,j}$. The onsite energies of each dot and tunnel couplings t_{lc} and t_{cr} between dots can be controlled electrically. The Hamiltonian is given by

$$H_{\text{fm},2} = \left[\frac{J}{4} (\boldsymbol{\sigma}_1 \cdot \boldsymbol{\sigma}_2 - 1) + \frac{1}{2} \mathbf{B}_c \cdot \boldsymbol{\sigma}_1 \right] \frac{1 - \tau_z}{2} + \left[\delta + \frac{1}{2} \mathbf{B}_l \cdot \boldsymbol{\sigma}_1 \right] \frac{1 + \tau_z}{2} + t_{lc} \tau_x + \frac{1}{2} \mathbf{B}_r \cdot \boldsymbol{\sigma}_2, \quad (2)$$

where $\mathbf{S}_i = \frac{1}{2} \boldsymbol{\sigma}_i$ are the spins of the two electrons ($\hbar = 1$, $i = 1, 2$) and J is the exchange interaction between dots 1 and 2, see Fig. 1(b). The onsite energies can be chosen, such that the charge configurations (1, 0, 1) and (0, 1, 1) are detuned by a controllable detuning $\delta \ll U_1$, where U_1 is the next-neighbor Coulomb repulsion. A third charge configuration (1, 1, 0), as well as charge configurations comprising double occupation of dots, are energetically separated by either U_1 or the on-site Coulomb energy, and are thus neglected. The system operates near the (0, 1, 1) \leftrightarrow (1, 0, 1) charge transition. Away from the charge transition, i.e., for $\delta \gg |t_{lc}|$, the system is in the (0, 1, 1) charge state and the electron spins couple with the exchange interaction J . This charge state corresponds to a ST_0 qubit next to an empty dot. Inside the charge transition regime, i.e. for $|\delta| \ll |t_{lc}|$, the charge states hybridize.

In the singlet-triplet basis of the two-spin subspace, the Hamiltonian Eq. (2) restricted to the computational ST_0 subspace is found to be

$$H_{\text{sys}} = \frac{\delta + J/2}{2} \tau_z + t_{lc} \tau_x + \frac{B_{l,z} - B_{c,z}}{4} \tilde{\sigma}_x \tau_z + \frac{B_{l,z} + B_{c,z} - 2B_{r,z}}{4} \tilde{\sigma}_x + \frac{J}{2} \tilde{\sigma}_z \frac{1 - \tau_z}{2}, \quad (3)$$

where the spin operators $\tilde{\sigma}_z$ and $\tilde{\sigma}_x$ act on the singlet and triplet states $|S\rangle = (|\uparrow\downarrow\rangle - |\downarrow\uparrow\rangle)/\sqrt{2}$ and $|T_0\rangle = (|\uparrow\downarrow\rangle + |\downarrow\uparrow\rangle)/\sqrt{2}$ as $\tilde{\sigma}_z |S\rangle = -|S\rangle$ and $\tilde{\sigma}_z |T_0\rangle = |T_0\rangle$. In the following, we define the gradient fields

$$\frac{\Delta b}{2} = \frac{B_{l,z} - B_{c,z}}{4}, \quad (4)$$

$$\frac{\Delta B}{2} = \frac{B_{l,z} + B_{c,z} - 2B_{r,z}}{4}. \quad (5)$$

Analogously to the flopping-mode qubit, the two low-energy charge states are coupled to the electric field of the microwave cavity mode $H_c = \omega_c a^\dagger a$ via the electric-dipole Hamiltonian

$$H_I = g_c \tau_z (a + a^\dagger), \quad (6)$$

where g_c is the charge-photon coupling. In the following, we set $g_c = 0.5 \mu\text{eV} = 120 \text{ MHz}$. The cavity-qubit system is depicted in Fig. 2. The cavity has two ports, port 1 and port 2, that are described by their photon-loss rates κ_1 and κ_2 , and the total decay rate is defined as $\kappa = \kappa_1 + \kappa_2 + \kappa_{\text{int}}$ with κ_{int} the internal photon loss. A probe field [51] with frequency ω_r defined with the Hamiltonian

$$H_p = i\sqrt{\kappa_1} (a_{\text{in}} e^{-i\omega_r t} a^\dagger + a_{\text{in}}^* e^{i\omega_r t} a) \quad (7)$$

can be applied at port 1 (which we define to be the input port). In summary, the entire cavity-qubit system is thus described by the Hamiltonian

$$H = H_{\text{sys}} + H_c + H_I + H_p. \quad (8)$$

III. EFFECTIVE HAMILTONIAN

We diagonalize the charge part $(\delta + J/2)\tau_z/2 + t_{lc}\tau_x$ of the Hamiltonian Eq. (3) to obtain the charge eigenenergies $\Omega = \pm\sqrt{(\delta + J/2)^2 + 4t_{lc}^2}/2$. Next, a Schrieffer-Wolff transformation is applied to H , projecting on the low-energy charge sector. The resulting perturbation theory is valid in the regime $g_c \ll \Delta b, J \ll \Omega$ where terms of order $O(g_c^2/\Omega)$ can be neglected. Note that H_p is invariant under that transformation. The resulting effective Hamiltonian is given by

$$H_{\text{eff}} = \left[\frac{J_{\text{eff}}}{2} + g_z (a + a^\dagger) \right] \tilde{\sigma}_z + \left[\frac{b_{\text{eff}}}{2} + g_x (a + a^\dagger) \right] \tilde{\sigma}_x + \omega_c a^\dagger a + H_p. \quad (9)$$

The dispersive shift and corrections due to vacuum fluctuations are of order g_c^2 and are thus neglected here. The Pauli matrices $\hat{\sigma}_x$ and $\hat{\sigma}_z$ act on the dressed spin states. The terms J_{eff} and b_{eff} are the effective qubit parameters which are given by

$$\begin{aligned} J_{\text{eff}} &= \frac{J}{2}(1 + \sin \theta) \\ &+ \frac{J^3}{4} \frac{\cos^2 \theta \sin \theta}{J^2 \sin^2 \theta - 4\Omega^2} + J\Delta b^2 \frac{\cos^2 \theta}{J^2 - 4\Omega^2}, \\ b_{\text{eff}} &= -\Delta b_{lc} \sin \theta + \Delta B \\ &+ \Delta b_{lc} \cos^2 \theta \frac{J^2(\sin \theta - 1)(4\Omega^2 + J^2 \sin \theta)}{2(J^2 - 4\Omega^2)(J^2 \sin^2 \theta - 4\Omega^2)}, \end{aligned} \quad (10)$$

with the orbital mixing angle $\theta = \arctan[(\delta + J/2)/2t_{lc}]$. To predict cavity transmissions in Section IV for $\omega_c \gtrsim 15 \mu\text{eV} \approx 3.6 \text{ GHz}$, second-order energy corrections have to be considered, see Appendix D. In addition to the renormalized qubit parameters, we find an effective transversal spin-photon coupling g_x and a longitudinal effective spin photon coupling g_z , both of the order g_c/Ω ,

$$\begin{aligned} g_x &= -\frac{\Delta b_{lc}}{2} g_c \cos(\theta)^2 \\ &\times \left(\frac{4\Omega}{J^2 - 4\Omega^2} - \frac{4\Omega}{(2\omega_c + J \sin(\theta))^2 - 4\Omega^2} \right), \\ g_z &= \frac{1}{8} J g_c \cos(\theta)^2 \left(\frac{4\Omega}{4\Omega^2 - (2\omega_c + J \sin(\theta))^2} \right. \\ &\left. + \frac{4\Omega}{4\Omega^2 - (2\omega_c - J \sin(\theta))^2} + \frac{8\Omega}{4\Omega^2 - J^2 \sin(\theta)^2} \right). \end{aligned} \quad (11)$$

Unlike the flopping-mode qubit that comprises only transversal coupling in its proposed operating regime [31], the singlet-triplet flopping-mode qubit thus inherits the observed ability of the ST qubit to couple longitudinally [28]. We predict strong longitudinal couplings with the possibility that $g_z > g_x$ in the operating regime of our model, thus exceeding the transversal coupling. Both couplings are plotted in Fig. 3. The couplings are highly tunable, with $g_x/g_c, g_z/g_c \rightarrow 0$ for $\delta \gg |t_{lc}|$.

IV. CAVITY TRANSMISSION

A. Input-output theory

To extract the couplings from the cavity transmission we use input-output theory [25, 59]. The goal is to calculate the cavity transmission $T = |\langle a_{\text{out},2} \rangle / \langle a_{\text{in},1} \rangle|^2$ in the quasistatic limit, thus the ratio of the output signal $\langle a_{\text{out},2} \rangle$ at port 2 and the input signal of the probe field at port 1, $\langle a_{\text{in},1} \rangle$. The output signal is related to the cavity field via $a_{\text{out},2} = \sqrt{\kappa_2} a$. For this, we first diagonalize the 2×2 effective qubit Hamiltonian

$$H_{\text{qb}} = \frac{J_{\text{eff}}}{2} \sigma_z + \frac{b_{\text{eff}}}{2} \sigma_x, \quad (12)$$

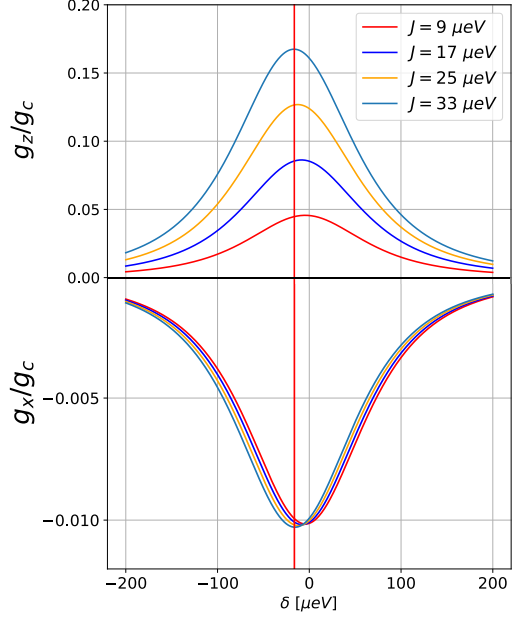


Figure 3. Cavity couplings g_z and g_x for the ST_0 flopping-mode qubit. The effective spin-photon couplings are plotted in units of g_c . Note the opposite sign of g_z and g_x . The coupling strengths are maximal if the qubit resonance is near $-\delta = J/2$, and decays as δ increases. At $\delta = -16.527 \mu\text{eV}$ (vertical red line) we obtain $g_z/g_c = 0.168$ and $g_x/g_c = -0.010$. Parameters used for the plot are $t_{lc} = 50 \mu\text{eV}$, $J = 33 \mu\text{eV}$, $B_{l,z} = 7 \mu\text{eV}$, $B_{c,z} = 5 \mu\text{eV}$, and $B_{r,z} = 2 \mu\text{eV}$.

and obtain the qubit energies

$$E_{0,1} = \pm \frac{1}{2} \sqrt{J_{\text{eff}}^2 + b_{\text{eff}}^2}, \quad (13)$$

with $E_1 > 0 > E_0$. Next, we solve the quantum Langevin equations for the system in the stationary limit, i.e., $t \rightarrow \infty$, such that $\dot{a} = \dot{\sigma}_{ij} = 0$, for $i, j \in \{0, 1\}$, with $\sigma_{ij} = |i\rangle \langle j|$. Here, $|i\rangle$, $i \in \{0, 1\}$ is the i th eigenstate of the effective qubit Hamiltonian (12). Applying a rotating wave approximation to remove the time dependence in H arising from the probe field, these equations become

$$\begin{aligned} 0 &= \dot{a} = -i[a, H_{\text{eff}}] \\ &= -i(\Delta_c a - g_{01} \sigma_{01} e^{i\omega_r t}) - \frac{\kappa}{2} a + \sqrt{\kappa_1} a_{\text{in},1}, \end{aligned} \quad (14)$$

and

$$\begin{aligned} 0 &= \dot{\tilde{\sigma}}_{01} = -i[\tilde{\sigma}_{01}, H_{\text{eff}}] \\ &= -i((E_1 - E_0 - \omega_r - i\gamma) \tilde{\sigma}_{01} + g_{01}(p_0 - p_1)a), \end{aligned} \quad (15)$$

with $\tilde{\sigma}_{01} = \sigma_{01} e^{i\omega_r t}$, $\Delta_c = \omega_r - \omega_c$, the thermal population $p_i = \langle \sigma_{ii} \rangle = \exp(-E_i/k_B T_{\text{dot}})$, $i = 0, 1$, and

$$g_{01} = g_x \frac{J_{\text{eff}}}{\sqrt{J_{\text{eff}}^2 + b_{\text{eff}}^2}} - g_z \frac{b_{\text{eff}}}{\sqrt{J_{\text{eff}}^2 + b_{\text{eff}}^2}}. \quad (16)$$

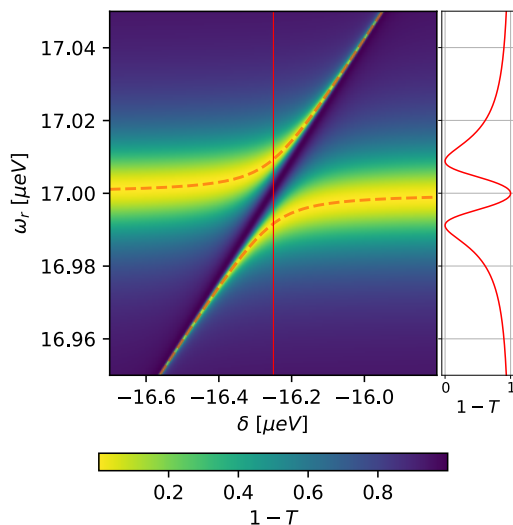


Figure 4. *Calculated cavity absorption $1 - T$ as a function of detuning δ and probe frequency ω_r .* Note the avoided crossing around the qubit resonance at $\delta = -16.257 \mu\text{eV} \approx -J/2$. The absorption spectrum is cut through the avoided crossing along the vertical red line to determine $1 - T(\omega_r)$, see the right panel. The distance between the two peaks indicates the vacuum Rabi splitting. The width of the avoided crossing is $2|g_{01}|\sqrt{p_0 - p_1} = 0.018 \mu\text{eV}$, resulting in $g_{01} = -0.025 \mu\text{eV}$, with $p_0 = 0.5653$ and $p_1 = 0.4346$. Parameters for the plot are $t_{lc} = 50 \mu\text{eV}$, $J = 33 \mu\text{eV}$, $B_{l,z} = 7 \mu\text{eV}$, $B_{c,z} = 5 \mu\text{eV}$ and $B_{r,z} = 2 \mu\text{eV}$. The resonator frequency is chosen as $\omega_c = 17 \mu\text{eV} = 4.1 \text{GHz}$.

In the following, we omit the tilde and set $T_{\text{dot}} = 0.75 \text{K}$. Considering the expectation values of a and σ_{01} we can rewrite Eq. (15) as

$$\langle \sigma_{01} \rangle = \chi(\omega_r) \langle a \rangle, \quad \chi(\omega_r) = \frac{-g_{01}(p_0 - p_1)}{E_1 - E_0 - \omega_r - i\gamma/2}. \quad (17)$$

The function χ is the electric susceptibility of the system [25], which encodes the qubit physics in the cavity transmission. In the following, we will neglect qubit dephasing and set $\gamma = 0$. Substituting this into (14) and again replacing a with its quasi-static expectation value, we find

$$T = \left| \frac{-i\sqrt{\kappa_1\kappa_2}}{\omega_c - \omega_r + g_{01}\chi - i\kappa/2} \right|^2. \quad (18)$$

B. Results

Both g_x and g_z can be extracted from the cavity transmission T by modulating the frequency of the drive field ω_r . At the resonance frequency $\omega_r = \omega_c$ we obtain absorption unless the qubit energy splitting is on resonance with the cavity, that is $\Delta E = E_1 - E_0 = \omega_c$. Then we find an avoided crossing in the cavity spectrum, and the minimal

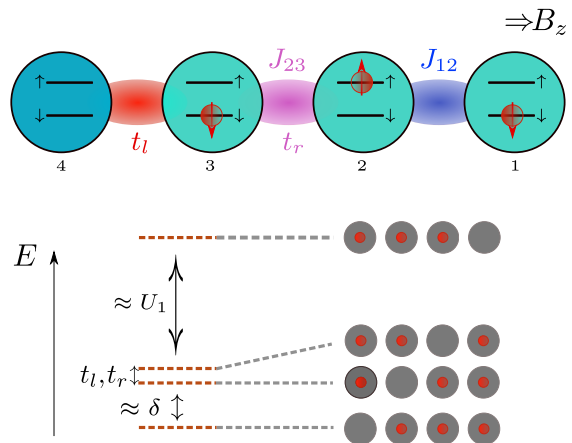


Figure 5. *Exchange-only flopping-mode spin qubit.* Top: Four QDs in a global magnetic field B_z . Dots 1, 2, and 3 form the EO qubit when dot 4 is far detuned. The exchange couplings J_{ij} between dots i and j and the tunnel couplings t_l between dots 3 and 4 and t_r between dots 2 and 3 control the qubit-cavity coupling and the qubit operation. Bottom: The four possible charge states without double occupation, organized according to their energy E . The state $(1, 1, 1, 0)$ is gapped out by $U_1 \gg \delta$. If $\delta \gg |t_l|, |t_r|$, the ground state is an EO qubit coupled to an empty dot and if $\delta \ll |t_l|$, the three low-lying charge states hybridize, enabling the spin-photon coupling.

width of the crossing (see Fig. 4) is $2g_{01}\sqrt{p_0 - p_1}$. The absorption $1 - T$ and a cross-section of the spectrum around the resonance of the qubit at $\delta + J/2 = -16.257 \mu\text{eV}$ are depicted in Fig. 4 for $t_{lc} = 50 \mu\text{eV}$, $J = 33 \mu\text{eV}$, $B_{l,z} = 7 \mu\text{eV}$, $B_{c,z} = 5 \mu\text{eV}$ and $B_{r,z} = 2 \mu\text{eV}$. The resonator frequency is chosen as $\omega_c/2\pi = 17 \mu\text{eV} = 4.1 \text{GHz}$. For $T = 0.75 \text{K}$ we have $p_0 = 0.565$ and $p_1 = 0.435$. For these parameters, we calculate $g_{01} = 0.018 \mu\text{eV}$. The coupling g_{01} depends on g_x and on g_z , see Eq. (16), and to extract these coupling parameters individually from the cavity output, a single cavity measurement is not sufficient. However, one can obtain g_x and g_z in two ways. One possibility is using that $g_x = 0$ for $\Delta b = 0$, so $g_z|_{\Delta b=0}$ can be resolved. By tuning Δb , one can then use the resolved g_z and calculate g_x from the measurement. Since Δb can usually not be tuned in situ, this would require measurements across several devices and thus demands an otherwise very high similarity of the devices. Another way of resolving both couplings is by measuring the cavity phase $\phi = \arg(\langle a_{\text{out},2} \rangle / \langle a_{\text{in},1} \rangle)$ in addition to the transmission, see Fig. 9 in Appendix B, for the same parameters. We calculate $g_x/g_c = -0.010$ and $g_z/g_c = 0.168$ for this case.

The couplings for different J are plotted as a function of δ in Fig. 3. The two couplings can, in a parameter regime as the used one, have opposite signs. At the resonance $\delta - J/2 = 0$, the two charge states are degenerate, and we find, as for the flopping-mode qubit [38], maximal spin-photon couplings at this operating point.

V. EXCHANGE-ONLY FLOPPING-MODE QUBIT

We now apply our flopping-mode approach to the exchange-only (EO) qubit. The EO qubit can be realized with three QDs and three electrons, one in each dot [8, 9]. Analogously to the ST_0 qubit, we study the case where an additional, empty QD is tunnel coupled to the EO qubit. The treatment of the system is similar to the ST_0 case, thus we only highlight the distinct aspects in detail. We now have a model with four QDs, labeled 1 through 4, occupied with three electrons, see Fig. 5. A global magnetic field is applied to separate the two decoherence-free subspaces of the EO qubit (see below). The relevant independent parameters are now the exchange couplings J_{12} [J_{23}] between dots (1) and (2) [(2)and (3)] and the tunnel coupling t_l between dots 3 and 4. The tunnel coupling t_r between dots 2 and 3, and the exchange interaction J_{34} between dots 3 and 4, are related to these quantities via $J_{23} \propto t_r^2$ and $J_{34} \propto t_l^2$, see Fig. 5. As the ST_0 case, our EO model neglects high-energy terms due to onsite Coulomb repulsion of doubly-occupied dots U_{2j} , $j = 1, 2, 3, 4$. While the ST_0 flopping-mode qubit comprises one additional low-energy charge state, we find that the EO flopping-mode qubit comes with two additional charge states. The four low-energy charge configurations are $(1, 1, 1, 0)$, $(1, 1, 0, 1)$, $(1, 0, 1, 1)$, and $(0, 1, 1, 1)$, see Fig. 5. The configuration $(1, 1, 1, 0)$ can be neglected, as in the case of the $(1, 1, 0)$ charge state in the ST_0 flopping-mode qubit, because it is gapped out by the large nearest-neighbor Coulomb energy U_1 . Thus, three states remain, and if dot 4 is detuned by δ_{eo} , then the Hamiltonian of the flopping-mode EO qubit including charge and spin degrees of freedom can then be expressed as

$$\begin{aligned}
H_{\text{fm},3} = & \left[J_{12} \mathbf{S}_1 \cdot \mathbf{S}_2 + J_{23} \mathbf{S}_2 \cdot \mathbf{S}_3 - \frac{J_{12} + J_{23}}{4} \right] \\
& \times |0111\rangle \langle 0111| \\
& + \left[\delta_{eo} + J_{12} \mathbf{S}_1 \cdot \mathbf{S}_2 - \frac{J_{12}}{4} \right] |1011\rangle \langle 1011| \\
& + \left[\delta_{eo} + J_{34} \mathbf{S}_2 \cdot \mathbf{S}_3 - \frac{J_{34}}{4} \right] |1101\rangle \langle 1101| \\
& + t_r (|1101\rangle \langle 1011| + h.c.) \\
& + t_l (|1011\rangle \langle 0111| + h.c.),
\end{aligned} \tag{19}$$

where $\mathbf{S}_i = \frac{1}{2} \boldsymbol{\sigma}_i$ is the electron spin operator for electron i . The computational spin subspace of the EO qubit is spanned by the states $|S_{123} = \frac{1}{2}, S_{12} = 0, m\rangle$, and $|S_{123} = \frac{1}{2}, S_{12} = 1, m\rangle$, where $m = -1/2, 1/2$ denotes the projection of the total spin of the three particles S_{123} to the z -axis, and $S_{12} = 0, 1$ is the total spin quantum number of the first two electrons. The qubit states can

be written as

$$\begin{aligned}
S_{12} = 0 : |0\rangle &= |S\rangle |m\rangle, \\
S_{12} = 1 : |1\rangle &= \frac{1}{\sqrt{3}} \left(\sqrt{2} |T_{2m}\rangle | -m\rangle - |T_0\rangle |m\rangle \right),
\end{aligned} \tag{20}$$

where $|T_{2m=1}\rangle = |T_+\rangle = |\uparrow\uparrow\rangle$ and $|T_{2m=-1}\rangle = |T_-\rangle = |\downarrow\downarrow\rangle$ are the polarized triplet states of the first two spins. Each of the two subspaces with either $m = +1/2$ or $m = -1/2$ realizes a valid qubit encoding, however, they are degenerate in energy unless a global Zeeman field is applied to separate them. Because Eq. (19) does not mix this subspace with the remaining eigenstates, we restrict the Hamiltonian in Eq. (19) to the $m = +1/2$ or the $m = -1/2$ subspace and, by adding $(J_{12} + J_{23})/2$ to it, we obtain

$$\begin{aligned}
H_{\text{eo,comp}} = & \left[\frac{2J_{12} - J_{23}}{4} \sigma_z + \frac{2m\sqrt{3}J_{23}}{4} \sigma_x \right] |0111\rangle \langle 0111| \\
& + \left[\delta_{eo} + \beta + \frac{J_{12}}{2} \sigma_z \right] |1011\rangle \langle 1011| \\
& + \left[\delta_{eo} + \alpha + \frac{J_{34}}{4} (-\sigma_z + 2m\sqrt{3}\sigma_x) \right] |1101\rangle \langle 1101| \\
& + t_r (|1101\rangle \langle 1011| + h.c.) + t_l (|1011\rangle \langle 0111| + h.c.),
\end{aligned} \tag{22}$$

with $\alpha = (J_{12} + J_{23} - J_{34})/2$ and $\beta = J_{23}/2$. Here, the σ -Pauli matrices act on the $|0\rangle, |1\rangle$ states as $\sigma_z |0\rangle = -|0\rangle$ and $\sigma_z |1\rangle = |1\rangle$. Note, that the subspaces with $m = \pm 1/2$ differ only by the sign of the $\sqrt{3}$ terms. In the following analysis, we look at $m = +1/2$ (however, see below for a discussion of the subsystem encoding). The charge degree of freedom of the four dots couples to the electric field of a microwave cavity mode, similarly to the ST qubit (Fig. 2) with one additional dot. The coupling to the cavity field is achieved by coupling dot 4 to the voltage at the center conductor of the cavity. This varies the energy of the states in which dot 4 is occupied, which is modeled by,

$$H_I = g_c (a + a^\dagger) (|1011\rangle \langle 1011| + |1101\rangle \langle 1101|). \tag{23}$$

In addition, a probe field described previously in Eq. (7) can be injected into the cavity. Now we can proceed similarly to the singlet-triplet case in Section II and derive an effective qubit Hamiltonian. However, the situation is more complex as there is one more charge state to consider. We can write the energy configuration of the three charge states as

$$H_C = \begin{pmatrix} (1, 1, 0, 1) & (1, 0, 1, 1) & (0, 1, 1, 1) \\ \delta_{eo} + \alpha & t_r & 0 \\ t_r & \delta_{eo} + \beta & t_l \\ 0 & t_l & 0 \end{pmatrix}. \tag{24}$$

The energies of the charge states can be controlled by $\delta_{\text{eo}} \ll U_1 \lesssim U_{2j}$ as in the ST_0 case. If $\delta_{\text{eo}} + \beta \approx \delta_{\text{eo}} \gg |t_l|$, the charge configuration of the ground state is $(0, 1, 1, 1)$. In this regime, the system behaves asymptotically like the EO qubit, i.e., only the $|0111\rangle$ $\langle 0111|$ - terms in the Hamiltonian Eq. (22) govern the dynamics, thus the system then can be described by

$$H_{\text{eo}} = \frac{2J_{12} - J_{23}}{4}\sigma_z + \frac{\sqrt{3}J_{23}}{4}\sigma_x, \quad (25)$$

which is the triple-dot EO qubit Hamiltonian [60]. For $|\delta_{\text{eo}}| \ll |t_l|$, the charge states hybridize. For $|\delta_{\text{eo}}| \gg |t_l|$, the qubit decouples from the resonator, however, for $\delta_{\text{eo}} < 0$, as the charge ground state consists of a hybridization of $(1, 0, 1, 1)$ and $(1, 1, 0, 1)$, such that the EO qubit state is not the ground state anymore and becomes unstable. A suitable idle regime with uncoupled qubit and resonator is therefore $\delta_{\text{eo}} > 0$ and $\delta_{\text{eo}} \gg |t_l|$.

Now we proceed by diagonalizing the charge sector of Eq. (22), followed by a Schrieffer-Wolff transformation in the regime $g_c \ll J_{12}, J_{23} \ll |E_i - E_j|$ and $U_{24} \geq U_{2j}$, with $j = 1, 2, 3$, for all eigenvalues $E_i \neq E_j$ of H_C . Here, the U_{2j} for $j = 1, 2, 3, 4$ are the onsite Coulomb repulsion energies of the four dots. The resulting effective Hamiltonian is of the form

$$H_{\text{eff}} = \left[\frac{J_{\text{eff, eo}}}{2} + g_{z, \text{eo}}(a + a^\dagger) \right] \tilde{\sigma}_z + \left[\frac{j_{\text{eff, eo}}}{2} + g_{x, \text{eo}}(a + a^\dagger) \right] \tilde{\sigma}_x + \omega_c a^\dagger a. \quad (26)$$

The effective Hamiltonian Eq. (26), with parameters given in Appendix C, again consists of the effective qubit Hamiltonian and longitudinal and transversal spin-photon couplings $g_{z, \text{eo}}$ and $g_{x, \text{eo}}$. These couplings are dependent on the tunnel couplings as well as the detuning δ_{eo} . We find that, unlike in the ST_0 case, the maximal coupling strength is not necessarily reached where the charge states are degenerate. Rather, the tunnel couplings t_l and t_r can shift the maximum. The coupling strengths $g_{z, \text{eo}}$ and $g_{x, \text{eo}}$ as a function of δ_{eo} are plotted for $m = +1/2$ in Fig. 6. The subspace-specific term $2m\sqrt{3}$ appears as a prefactor in g_x , while g_z is independent of m . Thus, g_z is identical in both subspaces, and $g_x(m = 1/2) = -g_x(m = -1/2)$. We can therefore envision using the longitudinal coupling g_z to couple the *subsystem* qubit to the cavity, and to couple two subsystem qubits via the exchange of cavity photons.

We can use the cavity phase ϕ to resolve $g_{x, \text{eo}}$ and $g_{z, \text{eo}}$, as shown in Fig. 7 for $t_l = 50 \mu\text{eV}$, $J_{12} = 13 \mu\text{eV}$, $t_r = 25 \mu\text{eV}$ (thus $J_{23} = 13.8 \mu\text{eV}$). The resonator frequency is set to be $\omega_c = 11 \mu\text{eV} = 2.66 \text{ GHz}$. For $T = 0.75\text{K}$ we find $p_0 = 0.542$ and $p_1 = 0.458$. A phase jump of π is observed at the resonance. The two points where $\phi = 0$ are separated by $\Delta\omega_r = 2g_{01, \text{eo}}\sqrt{p_0 - p_1}$, and together with a fit to the cavity transmission over ω_r , shown in Fig. 10, $g_{x, \text{eo}}$ and $g_{z, \text{eo}}$ are extracted. For the given parameters, we find $2|g_{01, \text{eo}}|\sqrt{p_0 - p_1} = 0.0078 \mu\text{eV}$, thus $g_{01, \text{eo}} =$

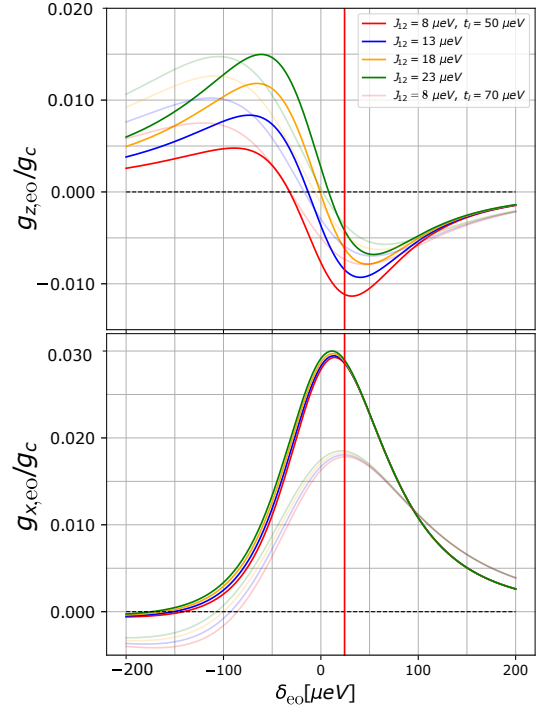


Figure 6. *Cavity couplings for the EO flopping-mode qubit.* The effective spin-photon couplings $g_{z, \text{eo}}/g_c$ and $g_{x, \text{eo}}/g_c$ for $t_l = 50 \mu\text{eV}$, $J_{12} = 13 \mu\text{eV}$, $t_r = 25 \mu\text{eV}$ (thus $J_{23} = 13.8 \mu\text{eV}$) as a function of δ_{eo} . The resonator frequency is $\omega_c = 11 \mu\text{eV} = 2.66 \text{ GHz}$. In that regime, the couplings have opposite signs. If $-\delta_{\text{eo}} \approx J_{12}/2$, g_z flips its sign. The couplings decay when $\delta_{\text{eo}} \gg |t_l|$. At $\delta_{\text{eo}} = 24.33 \mu\text{eV}$ (vertical red line) the cavity spectrum is being calculated, and there we obtain $g_{z, \text{eo}}/g_c = -0.0085$ and $g_{x, \text{eo}}/g_c = -0.029$.

$0.013 \mu\text{eV}$. The cavity transmission, which is plotted in Fig. 10 in Appendix B, can also be used to obtain $g_{01, \text{eo}}$. Calculating $g_{01, \text{eo}}$ from the effective parameters of Eq. (26) gives $g_{01, \text{eo}} = 0.013 \mu\text{eV}$, and this results in $g_{z, \text{eo}}/g_c = -0.0085$ and $g_{x, \text{eo}}/g_c = 0.029$. We see here, similar to the ST_0 flopping-mode qubit, that $g_{z, \text{eo}} < g_{x, \text{eo}}$. From Fig. 8 in Appendix C, we can see that $g_{01, \text{eo}} = 0$ at $\delta_{\text{eo}} \approx 90 \mu\text{eV}$ while $g_{x, \text{eo}}$ and $g_{z, \text{eo}}$ are each nonzero. At this spot, the qubit decouples from the cavity in the rotating wave approximation. However, the system is in a hybridized state of all three charge states. Opposing that, in the $\delta_{\text{eo}} \gg |t_l|$ regime in which the ground state charge configuration is $(0, 1, 1, 1)$, the EO qubit also decouples, resulting in $g_{01, \text{eo}} = g_{x, \text{eo}} = g_{z, \text{eo}} = 0$. The couplings do not vanish for $\delta_{\text{eo}}/|t_l| \rightarrow -\infty$. This can be explained by observing that in the regime $\delta_{\text{eo}}/|t_l| \rightarrow -\infty$, the ground state is a hybridization of the $(1, 0, 1, 1)$ and $(1, 1, 0, 1)$ charge states, which has a small residual electric dipole moment, comparable to that of the ST_0 flopping-mode qubit.

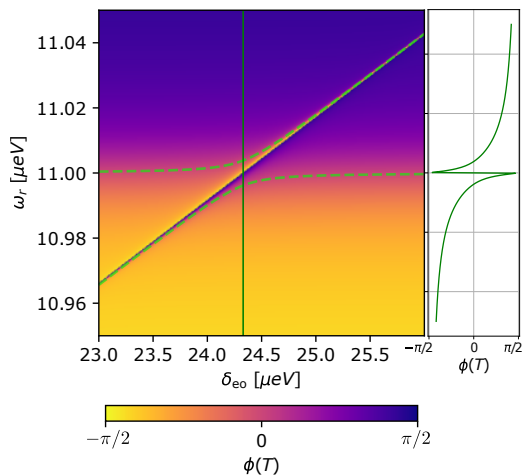


Figure 7. *Cavity phase spectrum for the EO flopping-mode qubit.* The cavity phase ϕ for $t_l = 50 \mu\text{eV}$, $J_{12} = 13 \mu\text{eV}$, $t_r = 25 \mu\text{eV}$ (thus $J_{23} \approx 13.8 \mu\text{eV}$). The resonator frequency is $\omega_c = 11 \mu\text{eV}$, $p_0 = 0.542$ and $p_1 = 0.458$. Around the qubit resonance at $\delta_{\text{eo}} = 24.33 \mu\text{eV}$, we find a π phase jump from $-\pi/2$ to $\pi/2$. The vertical green line gives $\phi(\omega_r)$ at the resonance. The distance of the points with $\phi = 0$ next to the phase jump is $2g_{01,\text{eo}}\sqrt{p_0 - p_1} = 0.0077 \mu\text{eV}$, thus $|g_{01,\text{eo}}| = 0.0132 \mu\text{eV}$, where $p_0 = 0.542$ and $p_1 = 0.458$.

VI. SUMMARY

The flopping-mode qubit adds a charge degree of freedom to the LD qubit, to enable the coupling to a resonator as well as low-power fast single-qubit gates. We combine this idea with the ST and EO qubit concepts by proposing to add a tunnel-coupled empty QD to the ST_0 and the EO qubits. We derive an effective Hamiltonian of the emerging singlet-triplet and exchange-only flopping-mode spin qubits. The resulting spin-photon coupling of these systems is investigated and highly tunable longitudinal and transversal couplings are found. By using input-output theory, the cavity transmission and phase are calculated, and the couplings are extracted from the transmission and phase spectrum. The tunable interactions allow for electrically controllable spin-photon couplings for the ST_0 and EO spin qubits in the low-energy charge regime. These represent promising steps to realize cavity-mediated baseband-controlled two-qubit interactions for ST_0 and EO spin qubits, which are locally quite challenging to realize. In addition, the longitudinal coupling is not dispersive and hence not subject to the Purcell effect. This may increase qubit lifetimes [28]. In the future, one can extend this analysis and enhance other qubits such as the four-spin singlet-only EO qubit to become ‘flopping mode’. Here we have focused on calculating and extracting the qubit-cavity couplings. From here on, one can apply known properties of the flopping-mode qubit [61, 62] to realize a readout protocol and qubit-qubit coupling for the new qubit flavors which are desired for

realizing larger quantum arrays of semiconductor qubits with long-range cavity-mediated couplings.

VII. ACKNOWLEDGMENTS

This work has been supported by the Army Research Office Grant No. W911NF-23-1-0104.

Appendix A: Combined coupling parameter

In this section, we define and plot the coupling parameter $g_{01,\text{eo}}$ (see Fig. 8) as it appears in Section V, in the cavity transmission and phase for the flopping-mode EO qubit. The coupling $g_{01,\text{eo}}$ is a combination of the longitudinal and transversal spin-couplings and the effective EO flopping-mode qubit parameters,

$$g_{01,\text{eo}} = g_{x,\text{eo}} \frac{J_{\text{eff},\text{eo}}}{\sqrt{J_{\text{eff},\text{eo}}^2 + j_{\text{eff},\text{eo}}^2}} - g_{z,\text{eo}} \frac{j_{\text{eff},\text{eo}}}{\sqrt{J_{\text{eff},\text{eo}}^2 + j_{\text{eff},\text{eo}}^2}}. \quad (\text{A1})$$

To decouple the EO qubit from the cavity, $g_{01,\text{eo}} \rightarrow 0$, one would choose $\delta_{\text{eo}} \gg |t_l|$. Note that for typical parameters t_l , t_r , and J_{12} , the total coupling $g_{01,\text{eo}}$ vanishes around $\delta = -100 \mu\text{eV}$. Therefore, within the rotating wave approximation, at this point, the qubit can be decoupled from the cavity in addition to the case $\delta/|t_l| \rightarrow \infty$. However, at the operating point with $\delta < 0$, the EO qubit exists in an excited charge state that can decay to a lower-energy state.

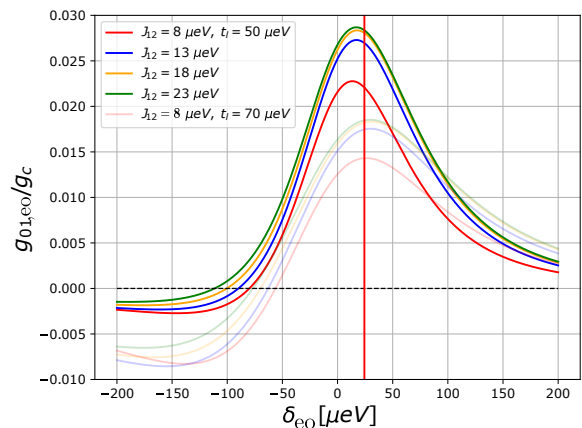


Figure 8. *The coupling parameter $g_{01,\text{eo}}$ as a function of δ_{eo} .* The parameters used for this plot are $t_l = 50 \mu\text{eV}$, $J_{12} = 13 \mu\text{eV}$, $t_r = 25 \mu\text{eV}$ (thus $J_{23} = 13.8 \mu\text{eV}$) over δ_{eo} . The resonator frequency is $\omega_c = 11 \mu\text{eV} = 2.66 \text{ GHz}$. The coupling decays for $\delta_{\text{eo}} \gg |t_l|$. At $\delta_{\text{eo}} = 24.33 \mu\text{eV}$ (vertical red line), the cavity spectrum is calculated, and we obtain $g_{z,\text{eo}}/g_c = -0.0085$ and $g_{x,\text{eo}}/g_c = -0.029$.

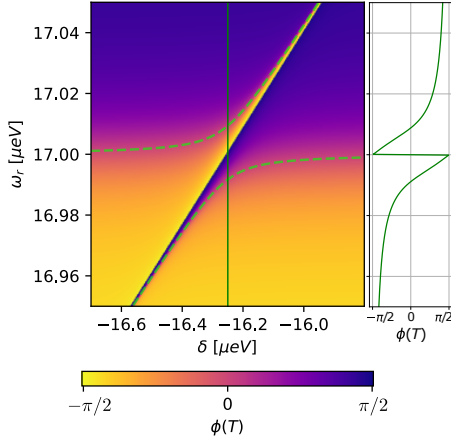


Figure 9. *Cavity phase spectrum of the ST_0 flopping-mode qubit.* The cavity phase ϕ for $t_{lc} = 50 \mu\text{eV}$, $J = 33 \mu\text{eV}$, $B_{l,z} = 7 \mu\text{eV}$, $B_{c,z} = 5 \mu\text{eV}$ and $B_{r,z} = 2 \mu\text{eV}$. The resonator frequency is $\omega_c = 17 \mu\text{eV}$. Around the qubit resonance at $\delta = -16.257 \mu\text{eV}$, thus $\delta + J/2 \approx 0$, we find a π -phase jump. The spectrum is cut through the avoided crossing along the vertical red line to determine $\phi(\omega_r)$. The distance between the two points with $\phi = 0$ each side of the phase jump is $2|g_{01}|\sqrt{p_0 - p_1} = 0.0180 \mu\text{eV}$ thus $g_{01} = -0.0246 \mu\text{eV}$.

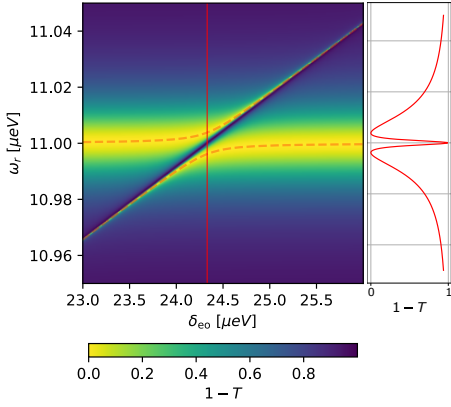


Figure 10. *Cavity absorption spectrum for the EO flopping-mode qubit.* The cavity absorption $1-T$ for $t_l = 50 \mu\text{eV}$, $J_{12} = 13 \mu\text{eV}$, $t_r = 25 \mu\text{eV}$ (thus $J_{23} \approx 13.8 \mu\text{eV}$). The resonator frequency is $\omega_c = 11 \mu\text{eV}$. Around the qubit resonance at $\delta_{\text{eeo}} = 24.33 \mu\text{eV}$, we find an avoided crossing. The vertical red line gives $1 - T(\omega_r)$ at the resonance. The width of the avoided crossing is $2g_{01,\text{eo}}\sqrt{p_0 - p_1} = 0.0077 \mu\text{eV}$ thus $|g_{01,\text{eo}}| = 0.0132 \mu\text{eV}$.

Appendix B: Transmission phase (modulus) of the ST_0 (EO) qubit

We plot the transmission phase ϕ for the ST_0 flopping-mode qubit in Fig. 9 for the parameters used in Sec-

tion IV B. In Fig. 10, we plot the absorption $1 - T$ for the EO flopping-mode qubit with the parameters used in Section V.

Appendix C: EO qubit effective parameters

In this section, we show the parameters of the effective Hamiltonian Eq. (26). We define

$$\begin{aligned} f &= -(\delta + \alpha)^2 + (\delta + \alpha)(\delta + \beta) - (\delta + \beta)^2 - 3(t_l^2 + t_r^2), \\ g &= 2(\delta + \alpha)^3 - 3(\delta + \alpha)^2(\delta + \beta) - 3(\delta + \alpha)(\delta + \beta)^2 \\ &\quad + 2(\delta + \beta)^3 - 18(\delta + \alpha)t_l^2 + 9(\delta + \beta)t_l^2 + 9(\delta + \alpha)t_r^2 \\ &\quad + 9(\delta + \beta)t_r^2, \\ h &= g + \sqrt{4f^3 + g^2}. \end{aligned} \quad (\text{C1})$$

Diagonalizing H_C leads to the charge eigenenergies, which we can write in a compact form with the cubic roots,

$$\begin{aligned} E_1 &= \frac{2\delta + \alpha + \beta}{3} - \frac{2^{1/3}f}{3h^{1/3}} + \frac{h^{1/3}}{3 \cdot 2^{1/3}}, \\ E_2 &= \frac{2\delta + \alpha + \beta}{3} + \frac{1 + i\sqrt{3}f}{3 \cdot 2^{2/3}h^{1/3}} - \frac{1 - i\sqrt{3}h^{1/3}}{6 \cdot 2^{1/3}}, \\ E_3 &= \frac{2\delta + \alpha + \beta}{3} + \frac{1 - i\sqrt{3}f}{3 \cdot 2^{2/3}h^{1/3}} - \frac{1 + i\sqrt{3}h^{1/3}}{6 \cdot 2^{1/3}}. \end{aligned} \quad (\text{C2})$$

The charge eigenstates are

$$\begin{aligned} \mathbf{v}_1 &= \left(\frac{-(\delta + \beta)E_1 + E_1^2 - t_l^2}{t_l t_r}, \frac{E_1}{t_l}, 1 \right), \\ \mathbf{v}_2 &= \left(\frac{-(\delta + \beta)E_2 + E_2^2 - t_l^2}{t_l t_r}, \frac{E_2}{t_l}, 1 \right), \\ \mathbf{v}_3 &= \left(\frac{-(\delta + \beta)E_3 + E_3^2 - t_l^2}{t_l t_r}, \frac{E_3}{t_l}, 1 \right). \end{aligned} \quad (\text{C3})$$

The normalized charge eigenstates are $\mathbf{n}_i = \mathbf{v}_i/|\mathbf{v}_i|$ and for $i, j = 1, 2, 3$ the j th component of \mathbf{n}_i is denoted as n_{ij} . We define

$$\xi_1 = \frac{1}{4}J_{34}(1 - n_{21}^2) - \frac{1}{2}J_{12}(n_{21}^2 + 1) + \frac{1}{4}J_{23}(1 - n_{23}^2), \quad (\text{C4})$$

$$\xi_2 = \frac{1}{4}J_{34}(1 - n_{11}^2) - \frac{1}{2}J_{12}(n_{11}^2 + 1) + \frac{1}{4}J_{23}(1 - n_{13}^2), \quad (\text{C5})$$

$$\xi_3 = \frac{J_{34} + 2J_{12}}{4}(n_{31}^2 - n_{11}^2) + \frac{1}{4}J_{23}(n_{33}^2 - n_{13}^2), \quad (\text{C6})$$

$$\xi_4 = \frac{J_{34} + 2J_{12}}{4}(n_{31}^2 - n_{21}^2) + \frac{1}{4}J_{23}(n_{33}^2 - n_{23}^2). \quad (\text{C7})$$

The effective transversal coupling is then,

$$\begin{aligned}
g_x = & \frac{2m}{8} \sqrt{3} n_{13} n_{33} g_c (J_{34} n_{11} n_{31} + J_{23} n_{13} n_{33}) \\
& \times \left(\frac{1}{E_1 - E_3 + \xi_3 - \omega} - \frac{1}{-E_1 + E_3 + \xi_3 - \omega} - \frac{1}{-E_1 + E_3 + \xi_1} + \frac{1}{E_1 - E_3 + \xi_1} \right) \\
& + \frac{2m}{8} \sqrt{3} n_{23} n_{33} g_c (J_{34} n_{21} n_{31} + J_{23} n_{23} n_{33}) \\
& \times \left(\frac{1}{E_2 - E_3 + \xi_4 - \omega} - \frac{1}{-E_2 + E_3 + \xi_4 - \omega} - \frac{1}{-E_2 + E_3 + \xi_2} + \frac{1}{E_2 - E_3 + \xi_2} \right).
\end{aligned} \tag{C8}$$

The effective longitudinal coupling can be written as,

$$\begin{aligned}
g_z = & \frac{g_c}{16} (n_{13} n_{33}) ((J_{34} + 2J_{12}) n_{11} n_{31} + J_{23} n_{13} n_{33}) \left(\frac{2}{-E_1 + E_3 - \xi_3} - \frac{1}{E_1 - E_3 + \xi_3 - \omega} \right. \\
& \left. + \frac{1}{-E_1 + E_3 - \xi_3 - \omega} \right) \\
& - \frac{g_c}{16} (n_{23} n_{33}) \left(n_{21} n_{31} \left(\frac{J_{34}}{4} + \frac{J_{12}}{2} \right) + n_{23} n_{33} \frac{J_{23}}{4} \right) \left(-\frac{2}{-E_2 + E_3 - \xi_4} + \frac{1}{E_2 - E_3 + \xi_4 - \omega} \right. \\
& \left. - \frac{1}{-E_2 + E_3 - \xi_4 - \omega} \right) - (\xi_i \leftrightarrow -\xi_i, \omega \leftrightarrow -\omega),
\end{aligned} \tag{C9}$$

where $(\xi_i \leftrightarrow -\xi_i, \omega \leftrightarrow -\omega)$ is defined as the same expression again but with ω and ξ_i replaced by $-\omega$ and $-\xi_i$ for $i = 1, 2, 3, 4$. The effective qubit parameters are

$$\begin{aligned}
j_{\text{eff, eo}} = & m\sqrt{3} (J_{34} n_{31}^2 + J_{23} n_{33}^2) + \frac{m\sqrt{3}}{2} \left[\left(-\frac{1}{4} J_{34} n_{11} n_{31} + \frac{1}{2} J_{12} n_{12} n_{32} + \left(\frac{J_{12}}{2} - \frac{J_{23}}{4} \right) n_{13} n_{33} \right) \right. \\
& \times (J_{34} n_{11} n_{31} + J_{23} n_{13} n_{33}) \left(-\frac{1}{E_1 - E_3 + \xi_3} + \frac{1}{-E_1 + E_3 + \xi_1} - \frac{1}{-E_1 + E_3 + \xi_3} + \frac{1}{E_1 - E_3 + \xi_1} \right) \\
& + \left(\frac{1}{4} J_{34} n_{21} n_{31} - \frac{1}{2} J_{12} n_{22} n_{32} - \left(\frac{J_{12}}{2} + \frac{J_{23}}{4} \right) n_{23} n_{33} \right) \\
& \left. \times (J_{34} n_{21} n_{31} + J_{23} n_{23} n_{33}) \left(\frac{1}{E_2 - E_3 + \xi_4} - \frac{1}{-E_2 + E_3 + \xi_2} + \frac{1}{-E_2 + E_3 + \xi_4} - \frac{1}{E_2 - E_3 + \xi_2} \right) \right],
\end{aligned} \tag{C10}$$

and

$$\begin{aligned}
J_{\text{eff, eo}} = & -\frac{1}{2} J_{34} n_{31}^2 + J_{12} n_{32}^2 + \left(J_{12} - \frac{J_{23}}{2} \right) n_{33}^2 \\
& + \left[\left(-\frac{1}{2} J_{12} n_{11} n_{31} - \frac{1}{4} J_{34} n_{11} n_{31} - \frac{1}{4} J_{23} n_{13} n_{33} \right)^2 \frac{1}{-E_1 + E_3 - \xi_3} \right. \\
& + \frac{3}{16} (J_{34} n_{11} n_{31} + J_{23} n_{13} n_{33})^2 \frac{1}{-E_1 + E_3 - \xi_1} \\
& + \left(\frac{1}{2} J_{12} n_{21} n_{31} + \frac{1}{4} J_{34} n_{21} n_{31} + \frac{1}{4} J_{23} n_{23} n_{33} \right)^2 \frac{1}{-E_2 + E_3 - \xi_4} \\
& \left. + \frac{3}{16} (J_{34} n_{21} n_{31} + J_{23} n_{23} n_{33})^2 \frac{1}{-E_2 + E_3 - \xi_2} - (\xi_i \leftrightarrow -\xi_i) \right].
\end{aligned} \tag{C11}$$

Appendix D: Second order energy contributions to the ST_0 flopping-mode qubit

The second-order energy contributions are given as,

$$\begin{aligned}
J_{\text{eff}}^2 = & \frac{J \cos \theta^2 (16\Delta b_{lc} (\Delta b_{lc} - B) \Omega^2 - \sin \theta (4\Delta b_{lc} \Delta B J^2 + J^4 + 16\Delta b_{lc}^2 \Omega^2 - 4J^2 \Omega^2 + 8\Delta b_{lc}^2 J^2 \sin \theta))}{2(J^2 - 4\Omega^2)(J^2 \sin^2 \theta - 4\Omega^2)}, \\
b_{\text{eff}}^2 = & \frac{\cos \theta^2 (4(\Delta b_{lc} - \Delta B) J^2 \Omega^2 + \Delta b_{lc} \sin \theta (4\Delta b_{lc} \Delta B J^2 + J^4 + 16\Delta b_{lc}^2 \Omega^2 - 4J^2 \Omega^2 - 2J^4 \sin \theta))}{(J^2 - \Omega^2)(J^2 \sin^2 \theta - 4\Omega^2)}.
\end{aligned} \tag{D1}$$

-
- [1] D. Loss and D. P. DiVincenzo, Quantum computation with quantum dots, *Phys. Rev. A* **57**, 120 (1998).
- [2] M. Veldhorst, J. Hwang, C. Yang, A. Leenstra, B. de Ronde, J. Dehollain, J. Muhonen, F. Hudson, K. M. Itoh, A. Morello, *et al.*, An addressable quantum dot qubit with fault-tolerant control-fidelity, *Nature Nanotechnology* **9**, 981 (2014).
- [3] A. M. Tyryshkin, S. Tojo, J. J. Morton, H. Riemann, N. V. Abrosimov, P. Becker, H.-J. Pohl, T. Schenkel, M. L. Thewalt, K. M. Itoh, *et al.*, Electron spin coherence exceeding seconds in high-purity silicon, *Nature Materials* **11**, 143 (2012).
- [4] Y.-H. Wu, L. C. Camenzind, A. Noiri, K. Takeda, T. Nakajima, T. Kobayashi, C.-Y. Chang, A. Sammak, G. Scappucci, H.-S. Goan, *et al.*, Hamiltonian phase error in resonantly driven cnot gate above the fault-tolerant threshold, *npj Quantum Information* **10**, 8 (2024).
- [5] B. E. Kane, A silicon-based nuclear spin quantum computer, *Nature* **393**, 133 (1998).
- [6] J. Levy, Universal quantum computation with spin-1/2 pairs and heisenberg exchange, *Phys. Rev. Lett.* **89**, 147902 (2002).
- [7] J. R. Petta, A. C. Johnson, J. M. Taylor, E. A. Laird, A. Yacoby, M. D. Lukin, C. M. Marcus, M. P. Hanson, and A. C. Gossard, Coherent manipulation of coupled electron spins in semiconductor quantum dots, *Science* **309**, 2180 (2005).
- [8] D. P. DiVincenzo, D. Bacon, J. Kempe, G. Burkard, and K. B. Whaley, Universal quantum computation with the exchange interaction, *Nature* **408**, 339 (2000).
- [9] B. H. Fong and S. M. Wandzura, Universal quantum computation and leakage reduction in the 3-qubit decoherence free subsystem, *Quantum Information and Computation* **11**, 1003 (2001).
- [10] D. Bacon, J. Kempe, D. A. Lidar, and K. B. Whaley, Universal fault-tolerant quantum computation on decoherence-free subspaces, *Phys. Rev. Lett.* **85**, 1758 (2000).
- [11] J. Taylor, H.-A. Engel, W. Dür, A. Yacoby, C. Marcus, P. Zoller, and M. Lukin, Fault-tolerant architecture for quantum computation using electrically controlled semiconductor spins, *Nature Physics* **1**, 177 (2005).
- [12] J. M. Taylor, V. Srinivasa, and J. Medford, Electrically protected resonant exchange qubits in triple quantum dots, *Phys. Rev. Lett.* **111**, 050502 (2013).
- [13] J. Medford, J. Beil, J. M. Taylor, E. I. Rashba, H. Lu, A. C. Gossard, and C. M. Marcus, Quantum-dot-based resonant exchange qubit, *Phys. Rev. Lett.* **111**, 050501 (2013).
- [14] A. J. Weinstein, M. D. Reed, A. M. Jones, R. W. Andrews, D. Barnes, J. Z. Blumoff, L. E. Euliss, K. Eng, B. H. Fong, S. D. Ha, *et al.*, Universal logic with encoded spin qubits in silicon, *Nature* **615**, 817 (2023).
- [15] V. N. Ivanova-Rohling, N. Rohling, and G. Burkard, Discovery of an exchange-only gate sequence for cnot with record-low gate time using reinforcement learning, arXiv preprint arXiv:2402.10559 [10.48550/arXiv.2402.10559](https://arxiv.org/abs/2402.10559) (2024).
- [16] S. Bose, Quantum communication through an unmodulated spin chain, *Phys. Rev. Lett.* **91**, 207901 (2003).
- [17] S. Bose, Quantum communication through spin chain dynamics: an introductory overview, *Contemporary Physics* **48**, 13 (2007).
- [18] M. Friesen, A. Biswas, X. Hu, and D. Lidar, Efficient multiqubit entanglement via a spin bus, *Phys. Rev. Lett.* **98**, 230503 (2007).
- [19] A. Sigillito, M. Gullans, L. Edge, M. Borselli, and J. Petta, Coherent transfer of quantum information in a silicon double quantum dot using resonant swap gates, *npj Quantum Information* **5**, 110 (2019).
- [20] N. J. Craig, J. M. Taylor, E. A. Lester, C. M. Marcus, M. P. Hanson, and A. C. Gossard, Tunable nonlocal spin control in a coupled-quantum dot system, *Science* **304**, 565 (2004).
- [21] F. K. Malinowski, F. Martins, T. B. Smith, S. D. Bartlett, A. C. Doherty, P. D. Nissen, S. Fallahi, G. C. Gardner, M. J. Manfra, C. M. Marcus, *et al.*, Fast spin exchange across a multielectron mediator, *Nature Communications* **10**, 1196 (2019).
- [22] G. Burkard, T. D. Ladd, A. Pan, J. M. Nichol, and J. R. Petta, Semiconductor spin qubits, *Rev. Mod. Phys.* **95**, 025003 (2023).
- [23] T. A. Baart, M. Shafiei, T. Fujita, C. Reichl, W. Wegscheider, and L. M. K. Vandersypen, Single-spin CCD, *Nature Nanotechnology* **11**, 330 (2016).
- [24] T. Fujita, T. A. Baart, C. Reichl, W. Wegscheider, and L. M. K. Vandersypen, Coherent shuttle of electron-spin states, *npj Quantum Information* **3**, 22 (2017).
- [25] G. Burkard, M. J. Gullans, X. Mi, and J. R. Petta, Superconductor-semiconductor hybrid-circuit quantum electrodynamics, *Nature Reviews Physics* **2**, 129 (2020).
- [26] L. Childress, A. Sørensen, and M. D. Lukin, Mesoscopic cavity quantum electrodynamics with quantum dots, *Physical Review A* **69**, 042302 (2004).
- [27] G. Burkard and A. Imamoglu, Ultra-long-distance interaction between spin qubits, *Physical Review B* **74**, 041307 (2006).
- [28] C. Böttcher, S. Harvey, S. Fallahi, G. Gardner, M. Manfra, U. Vool, S. Bartlett, and A. Yacoby, Parametric longitudinal coupling between a high-impedance superconducting resonator and a semiconductor quantum dot singlet-triplet spin qubit, *Nature Communications* **13**, 4773 (2022).
- [29] M. Russ, F. Ginzel, and G. Burkard, Coupling of three-spin qubits to their electric environment, *Phys. Rev. B* **94**, 165411 (2016).
- [30] A. J. Landig, J. V. Koski, P. Scarlino, U. Mendes, A. Blais, C. Reichl, W. Wegscheider, A. Wallraff, K. Ensslin, and T. Ihn, Coherent spin-photon coupling using a resonant exchange qubit, *Nature* **560**, 179 (2018).
- [31] M. Benito, X. Croot, C. Adelsberger, S. Putz, X. Mi, J. R. Petta, and G. Burkard, Electric-field control and noise protection of the flopping-mode spin qubit, *Phys. Rev. B* **100**, 125430 (2019).
- [32] X. Croot, X. Mi, S. Putz, M. Benito, F. Borjans, G. Burkard, and J. R. Petta, Flopping-mode electric dipole spin resonance, *Phys. Rev. Res.* **2**, 012006 (2020).
- [33] M. Benito, J. R. Petta, and G. Burkard, Optimized cavity-mediated dispersive two-qubit gates between spin qubits, *Physical Review B* **100**, 081412 (2019).
- [34] A. Warren, E. Barnes, and S. E. Economou, Long-distance entangling gates between quantum dot spins mediated

- by a superconducting resonator, *Physical Review B* **100**, 161303 (2019).
- [35] X. Mi, J. Cady, D. Zajac, P. Deelman, and J. R. Petta, Strong coupling of a single electron in silicon to a microwave photon, *Science* **355**, 156 (2017).
- [36] X. Hu, Y.-x. Liu, and F. Nori, Strong coupling of a spin qubit to a superconducting stripline cavity, *Physical Review B* **86**, 035314 (2012).
- [37] X. Mi, M. Benito, S. Putz, D. M. Zajac, J. M. Taylor, G. Burkard, and J. R. Petta, A coherent spin-photon interface in silicon, *Nature* **555**, 599 (2018).
- [38] M. Benito, X. Mi, J. M. Taylor, J. R. Petta, and G. Burkard, Input-output theory for spin-photon coupling in si double quantum dots, *Phys. Rev. B* **96**, 235434 (2017).
- [39] F. Borjans, X. Croot, X. Mi, M. Gullans, and J. Petta, Resonant microwave-mediated interactions between distant electron spins, *Nature* **577**, 195 (2020).
- [40] P. Harvey-Collard, J. Dijkema, G. Zheng, A. Sammak, G. Scappucci, and L. M. Vandersypen, Coherent spin-spin coupling mediated by virtual microwave photons, *Physical Review X* **12**, 021026 (2022).
- [41] J. Dijkema, X. Xue, P. Harvey-Collard, M. Rimbach-Russ, S. L. de Snoo, G. Zheng, A. Sammak, G. Scappucci, and L. M. Vandersypen, Cavity-mediated iswap oscillations between distant spins, *Nature Physics* **21**, 168 (2024).
- [42] B. D’Anjou and G. Burkard, Optimal dispersive readout of a spin qubit with a microwave resonator, *Physical Review B* **100**, 245427 (2019).
- [43] K. Petersson, C. Smith, D. Anderson, P. Atkinson, G. Jones, and D. Ritchie, Charge and spin state readout of a double quantum dot coupled to a resonator, *Nano Letters* **10**, 2789 (2010).
- [44] J. Mielke, J. R. Petta, and G. Burkard, Nuclear spin readout in a cavity-coupled hybrid quantum dot-donor system, *PRX Quantum* **2**, 020347 (2021).
- [45] M. House, T. Kobayashi, B. Weber, S. Hile, T. Watson, J. Van Der Heijden, S. Rogge, and M. Simmons, Radio frequency measurements of tunnel couplings and singlet-triplet spin states in Si:P quantum dots, *Nature Communications* **6**, 8848 (2015).
- [46] J. Colless, A. Mahoney, J. Hornibrook, A. Doherty, H. Lu, A. Gossard, and D. Reilly, Dispersive readout of a few-electron double quantum dot with fast rf gate sensors, *Physical review letters* **110**, 046805 (2013).
- [47] C. X. Yu, S. Zihlmann, J. C. Abadillo-Uriel, V. P. Michal, N. Rambal, H. Niebojewski, T. Bedecarrats, M. Vinet, É. Dumur, M. Filippone, *et al.*, Strong coupling between a photon and a hole spin in silicon, *Nature Nanotechnology* **18**, 741 (2023).
- [48] R. L. Delva, J. Mielke, G. Burkard, and J. R. Petta, Measurement-based entanglement of semiconductor spin qubits, *Phys. Rev. B* **110**, 035304 (2024).
- [49] P. M. Mutter and G. Burkard, Natural heavy-hole flopping mode qubit in germanium, *Phys. Rev. Res.* **3**, 013194 (2021).
- [50] R.-Z. Hu, R.-L. Ma, M. Ni, Y. Zhou, N. Chu, W.-Z. Liao, Z.-Z. Kong, G. Cao, G.-L. Wang, H.-O. Li, and G.-P. Guo, Flopping-mode spin qubit in a Si-MOS quantum dot, *Applied Physics Letters* **122**, 134002 (2023).
- [51] F. Ginzler and G. Burkard, Proposal for a cavity-induced measurement of the exchange coupling in quantum dots, *Phys. Rev. Res.* **4**, 033048 (2022).
- [52] A. Blais, A. L. Grimsmo, S. M. Girvin, and A. Wallraff, Circuit quantum electrodynamics, *Reviews of Modern Physics* **93**, 025005 (2021).
- [53] N. Didier, J. Bourassa, and A. Blais, Fast quantum non-demolition readout by parametric modulation of longitudinal qubit-oscillator interaction, *Physical review letters* **115**, 203601 (2015).
- [54] P.-Q. Jin, M. Marthaler, A. Shnirman, and G. Schön, Strong coupling of spin qubits to a transmission line resonator, *Physical review letters* **108**, 190506 (2012).
- [55] S. Richer, N. Maleeva, S. T. Skacel, I. M. Pop, and D. DiVincenzo, Inductively shunted transmon qubit with tunable transverse and longitudinal coupling, *Physical Review B* **96**, 174520 (2017).
- [56] R. Ruskov and C. Tahan, Quantum-limited measurement of spin qubits via curvature couplings to a cavity, *Physical Review B* **99**, 245306 (2019).
- [57] R. Ruskov and C. Tahan, Modulated longitudinal gates on encoded spin qubits via curvature couplings to a superconducting cavity, *Physical Review B* **103**, 035301 (2021).
- [58] N. M. Estakhri, A. Warren, S. E. Economou, and E. Barnes, Long-distance photon-mediated and short-distance entangling gates in three-qubit quantum dot spin systems, *Phys. Rev. Res.* **6**, 043029 (2024).
- [59] C. W. Gardiner and M. J. Collett, Input and output in damped quantum systems: Quantum stochastic differential equations and the master equation, *Phys. Rev. A* **31**, 3761 (1985).
- [60] C.-Y. Hsieh, Y.-P. Shim, M. Korkusinski, and P. Hawrylak, Physics of lateral triple quantum-dot molecules with controlled electron numbers, *Reports on Progress in Physics* **75**, 114501 (2012).
- [61] F. Ginzler and G. Burkard, Simultaneous transient dispersive readout of multiple spin qubits, *Phys. Rev. B* **108**, 125437 (2023).
- [62] J. Mielke, J. R. Petta, and G. Burkard, Nuclear spin readout in a cavity-coupled hybrid quantum dot-donor system, *PRX Quantum* **2**, 020347 (2021).